PBE+U calculations of the Jahn-Teller effect in PrO_2

Fabien Tran, Johannes Schweifer, Peter Blaha, and Karlheinz Schwarz
Institute of Materials Chemistry, Vienna University of Technology, Getreidemarkt 9/165-TC, A-1060 Vienna, Austria

Pavel Novák
Institute of Physics, Academy of Sciences of the Czech Republic, Cukrovarnická 10, CZ-162 53 Prague 6, Czech Republic

(Received 30 October 2007; revised manuscript received 20 December 2007; published 28 February 2008)

The Jahn-Teller distortion in praseodymium dioxide (PrO_2) has been studied using density functional theory with the PBE+U functional for the exchange-correlation energy. Various possible distortions were suggested based on recent neutron diffraction experiments [C. H. Gardiner *et al.*, Phys. Rev. B **70**, 024415 (2004)]. We could identify the most likely distorted structure with a magnitude of the distortion in very good agreement with the experiment. This structure is the one with the lowest total energy and the corresponding calculated electronic and magnetic properties agree well with the experiment. We investigated the dependency of various properties on the Coulomb parameter $U_{\text{eff}}=U-J$ and suggest $U_{\text{eff}}=6$ eV as the most appropriate value, for which about 1.65 $4f$ electrons (one localized plus 0.65 delocalized) per Pr atom are found. We also show that magnetism (antiferromagnetism or ferromagnetism) has only a minor influence on the energy and magnitude of the distortion, which is consistent with the fact that the Néel temperature (13.5 K) is much smaller than the temperature of 120 K below which the distortion is observed.

DOI: 10.1103/PhysRevB.77.085123 PACS number(s): 71.15.Mb, 71.70.Ej, 71.20.Eh, 71.27.+a

I. INTRODUCTION

The compounds CeO_2, PrO_2, and TbO_2 are the only lanthanide dioxides which have been successfully synthesized. CeO_2 occurs naturally, while a positive oxygen pressure is necessary to form PrO_2 and TbO_2. Most of the other lanthanide oxides occur naturally as sesquioxides (Ln_2O_3) (see Refs. 1 and 2 for reviews on lanthanide oxides). From the theoretical point of view, Ce oxides have been extensively studied and papers reporting density functional theory[3,4] (DFT) calculations of the geometrical and electronic structures of CeO_2 and Ce_2O_3 have recently appeared.[5–11] From these studies, it became apparent that it is necessary to go beyond the local density approximation (LDA) or generalized gradient approximation (GGA) in order to accurately reproduce the experimental results of these two Ce oxides, in particular, for Ce_2O_3, for which the formal valence is Ce^{3+} (i.e., one $4f$ electron per Ce atom).

More generally, it is well known that LDA and GGA functionals usually lead to qualitatively wrong results when they are applied to solids containing localized electrons (e.g., transition-metal and lanthanide oxides). The main reason for this shortcoming is the self-interaction error (the electrostatic interaction of an electron with itself) that is contained in these approximate functionals and their associated potentials (functional derivative).[12] The LDA(GGA)+U method[13,14] (see, e.g., Refs. 5, 7, 9–11, and 15–18 for recent applications on systems containing lanthanides or actinides) and more recently the hybrid functionals[19,20] (see Refs. 8, 11, and 21–24 for studies on solids containing lanthanides or actinides) were shown to be efficient to improve the description of solids containing localized electrons. We also mention the self-interaction-corrected LDA functional[12] (SIC-LDA) which has been applied successfully to lanthanide-containing solids.[25–27]

In this work, we present the results of DFT calculations for PrO_2 which were obtained using the GGA+U functional[13,14] for the exchange-correlation energy, and for its GGA part, we chose the functional developed by Perdew, Burke, and Ernzerhof (PBE).[28] In particular, we will focus on the Jahn-Teller distortion which was recently observed and reported in Refs. 29–31 (see also Ref. 32) and show that the PBE+U functional is able to reproduce this distortion rather well. The undistorted PrO_2 is a cubic fluorite structure (CaF_2) with a lattice constant of 5.386 Å.[30] Several experiments have been devoted to PrO_2 concerning its electronic ground state, but different interpretations have emerged. Early neutron diffraction experiments by Kern *et al.*[33,34] determined the crystal field splitting between the Γ_8 ground state and the Γ_7 excited state of the $J=5/2$ multiplet to be 130 meV. They also found that the magnetic ordering is antiferromagnetic ($T_N=14$ K) but did not observe any lattice distortion.[33,34] Combining different x-ray spectroscopies with the Anderson impurity model, Kotani and co-workers[35–37] deduced that PrO_2 is a highly correlated and partly covalent oxide, which can be described by a mixing of Pr^{4+} and Pr^{3+} configurations (a $4f$ occupancy of 1.5–1.6 electrons is calculated). From reflectivity and resonant photoemission, Kimura *et al.*[38] observed the coexistence of the Pr^{4+} and Pr^{3+} states in $PrO_{2-\delta}$. From x-ray absorption spectroscopy, it was suggested in Refs. 39 and 40 that the ground state consists of one localized $4f$ electron (Pr^{4+} configuration) plus an additional delocalized state having some $4f$ character hybridized with O $2p$ states. More recently, it was deduced from neutron diffraction experiments that for 90% of the Pr atoms, the configuration is Pr^{4+} (Ref. 29) and that below the Néel temperature of $T_N=13.5$ K, PrO_2 has a complicated noncollinear magnetic structure which consists of two components,[30,31] with a magnetic moment on Pr of 0.65 ± 0.02 and 0.35 ± 0.04 μ_B, respectively. Previous experimental studies reported a total magnetic moment of 0.6 ± 0.1,[33] 0.572 ± 0.012,[41] and 0.68 ± 0.07 μ_B.[41] In Ref. 30, an activation energy of 0.262 eV for the conductivity was measured,

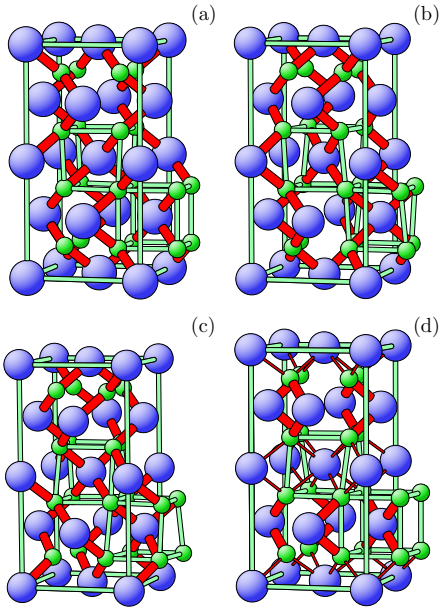

FIG. 1. (Color online) The four considered distorted structures: (a) JT1, (b) JT2, (c) JT3, and (d) JT4. The bigger (blue) spheres are the Pr atoms and the smaller (green) are the O atoms. Three types of Pr–O bonds occur, namely, a short (thick), an intermediate (thin), and a long (no bond shown) distance.

whereas a conducting behavior was reported in Ref. 42.

The number of DFT calculations on PrO_2 available in literature is rather small. Koelling *et al.*[43] reported the first calculation on PrO_2. They used LDA for the exchange-energy functional and neglected correlation. In Refs. 44 and 45, LDA calculations on PrO_2 were performed using the pseudopotential and tight-binding linear muffin-tin orbital methods, respectively. PrO_2 is among the numerous lanthanide oxides considered by Svane and co-workers[6,26,27] who used the SIC-LDA functional. Finally, we also mention the crystal field calculations for PrO_2 reported by Diviš and co-workers.[46–48] The DFT calculations presented in these cited papers were done assuming the perfect fluorite structure (in Ref. 45, the high-pressure α-$PbCl_2$ orthorhombic phase[49] was considered, too), i.e., none of them considered the Jahn-Teller distortion.

The paper is organized as follows. In Sec. II, the theoretical method is briefly outlined and the computational details are given. In Sec. III, we present the considered distorted structures, and in Sec. IV the results are discussed. Finally, in Sec. V, the conclusion is given.

II. THEORETICAL METHOD AND COMPUTATIONAL DETAILS

The calculations were done with the WIEN2K code[50–52] which is based on the full-potential (linearized) augmented plane-wave and local orbitals [FP-(L)APW+lo] method[53,54] to solve the Kohn-Sham equations[4] of DFT. The Brillouin zone integrations were performed with **k** meshes which were large enough to obtain well converged results. For instance, for calculations in a tetragonal unit cell (see Fig. 1) containing 8 f.u., a $10\times10\times5$ special point grid was used. $R_{\mathrm{MT}}^{\mathrm{min}}K_{\mathrm{max}}=7$ (the product of the smallest of the atomic sphere radii R_{MT} and the plane-wave cutoff parameter K_{max}) was used for the expansion of the basis set since test calculations with $R_{\mathrm{MT}}^{\mathrm{min}}K_{\mathrm{max}}=8$ led only to minor changes in the results. The sphere radii R_{MT} of Pr and O atoms were chosen as 2.5 and 1.7 a.u., respectively. The spin-orbit (SO) coupling was included in the calculations based on the second variational approach[55–57] using a basis set of states up to 60 eV above the Fermi energy. The inclusion of SO coupling was necessary in order to obtain a magnetic moment on the Pr atom (containing spin and orbital contributions) in good agreement with the experimental values (see Sec. IV). In addition to the symmetry lowering due to the distortion of the oxygen sublattice and antiferromagnetic ordering, a further symmetry lowering was sometimes (depending on the distorted structure) necessary in order to reach the lowest-energy state. For such systems, the lowering of symmetry can be necessary, and in Ref. 17 this aspect has been discussed in detail for lanthanide mononitrides. We should also mention that we neglected the noncollinearity of the magnetic structure of PrO_2,[30,31] which can be justified by the fact that the temperature $T_D=120$ K, below which the distortion is observed, is much larger than the Néel temperature $T_N=13.5$ K.[30,31] Nevertheless, we considered different collinear magnetic phases in order to study the influence of the magnetic structure on other properties (electronic structure and geometry).

Concerning the exchange-correlation energy, we chose the PBE+U functional

$$E_{\mathrm{xc}}^{\mathrm{PBE}+U}=E_{\mathrm{xc}}^{\mathrm{PBE}}+E_{\mathrm{ee}}-E_{\mathrm{dc}}, \tag{1}$$

where $E_{\mathrm{xc}}^{\mathrm{PBE}}$ is the nonempirical GGA functional developed by Perdew *et al.*,[28]

$$E_{\mathrm{ee}}=\frac{1}{2}\sum_{\sigma,\sigma'}\sum_{m_1,m_2,m_3,m_4} n_{m_1m_2}^{\sigma}n_{m_3m_4}^{\sigma'}(\langle m_1m_3|v_{\mathrm{ee}}^{s}|m_2m_4\rangle - \langle m_1m_3|v_{\mathrm{ee}}^{s}|m_4m_2\rangle\delta_{\sigma\sigma'}) \tag{2}$$

is an electron-electron (ee) interaction energy of Hartree-Fock-type[58] for the electrons of a selected atom and angular momentum ℓ, and

$$E_{\mathrm{dc}}=U\frac{n_\ell(n_\ell-1)}{2}-J\sum_{\sigma}\frac{n_\ell^{\sigma}(n_\ell^{\sigma}-1)}{2} \tag{3}$$

is the atomic limit version of the double-counting (dc) term.[59] In Eq. (2), $n_{m_im_j}^{\sigma}$ ($m_i=-\ell,\ldots,\ell$ and σ is the spin index) is the occupation matrix and v_{ee}^{s} is a screened Coulomb operator. In Eq. (3), $n_\ell=n_\ell^{\uparrow}+n_\ell^{\downarrow}$, where n_ℓ^{σ} is the total number of spin-σ electrons of angular momentum ℓ, and U and J [related to the integrals in Eq. (2) (Ref. 58)] are the screened Coulomb and exchange parameters, respectively, which are treated as empirical parameters or can be estimated by a constrained calculation.[60,61] Contrary to $E_{\mathrm{xc}}^{\mathrm{PBE}}$, E_{ee} is free of self-interaction errors (important for localized d and f electrons) and thus leads to a better description of the electrons of angular momentum ℓ. E_{dc} is subtracted to remove the interactions among these electrons contained in $E_{\mathrm{xc}}^{\mathrm{PBE}}$. Note that the calculations presented in this work were

TABLE I. The space groups and Wyckoff positions of the Pr and O atoms of the four considered PrO_2 distorted structures (see Figs. 1 and 2) without considering any magnetic order.

Structure	Space group	Pr Wyckoff positions	O Wyckoff positions
JT1	*Ibam* (No. 72)	$4a(0,0,\frac{1}{4})$, $4d(\frac{1}{2},0,0)$	$16k(\frac{1}{4},\frac{1}{4}+d,\frac{3}{8})$
JT2	$I4_1/acd$ (No. 142)	$8b(0,\frac{1}{4},\frac{1}{8})$	$16e(\frac{1}{4}+d,0,\frac{1}{4})$
JT3	$I4_1/acd$ (No. 142)	$8a(0,\frac{1}{4},\frac{3}{8})$	$16e(\frac{1}{4}+d,0,\frac{1}{4})$
JT4	$I4/mcm$ (No. 140)	$4a(0,0,\frac{1}{4})$, $4d(0,\frac{1}{2},0)$	$16l(\frac{1}{4}+\frac{d}{\sqrt{2}},\frac{1}{4}-\frac{d}{\sqrt{2}},\frac{1}{8})$

done with U replaced by $U_{\text{eff}}=U-J$ and $J=0$ in Eqs. (2) and (3), which leads to the simpler expression

$$E_{\text{ee}}-E_{\text{dc}}=\frac{U_{\text{eff}}}{2}\sum_{\sigma}\sum_{m_1}\left(n^{\sigma}_{m_1m_1}-\sum_{m_2}n^{\sigma}_{m_1m_2}n^{\sigma}_{m_2m_1}\right). \quad (4)$$

For details about the implementation of Eqs. (2) and (3) (and their associated potentials) within the FP-(L)APW+lo method, see Ref. 62. All calculations were done at the experimental lattice constant of 5.386 Å, which was determined by x-ray diffraction experiments at about 10 K.[30]

III. DISTORTED STRUCTURES

As mentioned in the Introduction, Gardiner *et al.*[30] reported a Jahn-Teller distortion below $T_D=120$ K. They performed neutron diffraction experiments on single crystals of PrO_2. Their data did not allow a unique structure determination but left several proposals for possible distorted structures of the oxygen sublattice (the praseodymium sublattice is undisturbed). In their models, the unit cell is doubled along one crystal axis and the distortion consists of displacing the oxygen atoms perpendicular to the direction along which the unit cell is doubled. The displacement from the ideal (fluorite structure) position is the same for all oxygen atoms, and thus only one parameter (d) is necessary to characterize it.

Two distorted structures are discussed in detail, whose space groups (without taking into account the lowering of symmetry due to an antiferromagnetic phase) and Wyckoff positions are indicated in Table I. The first one is JT1 [Fig. 1(a)], which leads to two inequivalent Pr atoms, whose first-neighboring atoms (oxygen cage) are shown in Figs. 2(a) and 2(b). The second distorted structure, called JT2, is shown in Fig. 1(b) and leads to Pr atoms which are all equivalent [the oxygen cage is Fig. 2(c)]. The JT2 structure corresponds to the structure shown in Fig. 8 of Ref. 30, but we should mention that in Ref. 30, it was indicated in the text that for JT2 structure the Pr atoms are at positions $8a(0,1/4,3/8)$ which are, however, not in accordance with their Fig. 8. Assuming the positions $8a(0,1/4,3/8)$ for the Pr atoms leads to structure JT3, which is shown in Fig. 1(c), and the corresponding oxygen cage in Fig. 2(d). Since we do not know which positions of the Pr atoms [$8b(0,1/4,1/8)$ or $8a(0,1/4,3/8)$] were actually favored by the authors,[30] we considered both JT2 and JT3 distorted structures for our calculations.

JT1 and JT2 (or JT3) are not the only structures which are consistent with the measured reflections. Gardiner *et al.*[30] also mentioned a structure that consists of a superposition of two JT1 distortions but with oxygen displacements in mutually perpendicular directions. For such a structure, the overall displacement of an oxygen atom is $d=\sqrt{2}\times 0.0511=0.0723$ Å. Therefore, we also considered two of such distorted structures. The first, called JT4 [Fig. 1(d) and Table I], leads to two inequivalent Pr sites, whose oxygen cages are shown in Figs. 2(e) and 2(f). The second structure we considered (not shown) led to no distortion; therefore, we will not consider it further in the present paper. Note that the difference between cages 2(a) and 2(f) is that for cage 2(a), there are two different O–O bond lengths among the O–O bonds parallel to the sheet plane, whereas for cage 2(f), all these O–O bonds have the same length. From Fig. 2, we can see that for cages 2(b) and 2(d), the four short Pr–O bonds form a tetrahedron, while for cages 2(a), 2(c), and 2(f), the four short Pr–O bonds are situated in a plane [only approximately for 2(c)]. In cage 2(e), all Pr–O bonds have the same length.

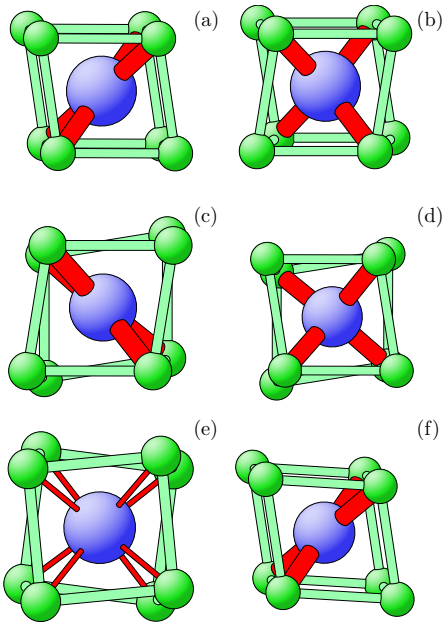

FIG. 2. (Color online) The different types of distorted oxygen cages found in structures (a)–(d) of Fig. 1. The bigger (blue) spheres are the Pr atoms and the smaller (green) are the O atoms. Three types of Pr–O bonds occur, namely, a short (thick), an intermediate (thin), and a long (no bond shown) distance. The displacements of the O atoms are parallel to the sheet plane and are exaggerated for clarity.

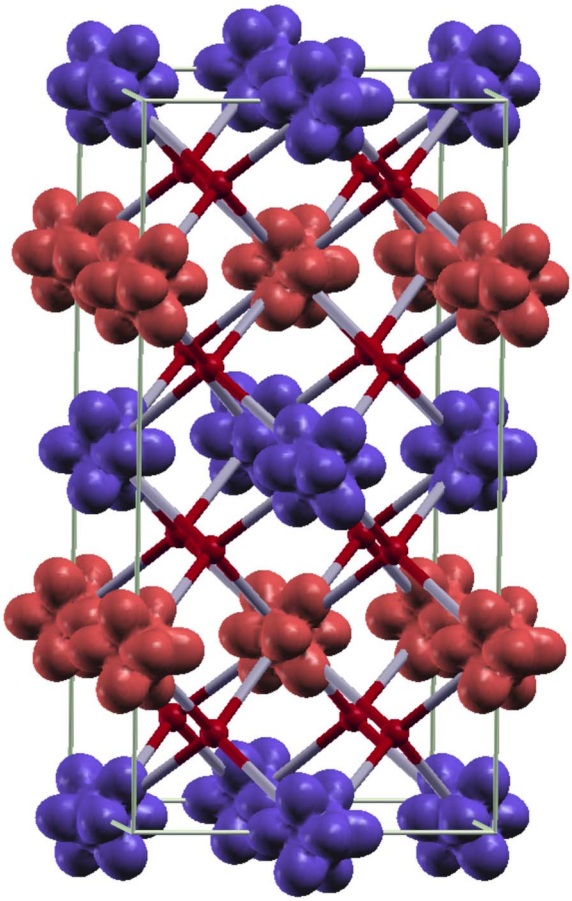

FIG. 3. (Color online) Isosurface of the spin magnetization density ($\rho_\uparrow - \rho_\downarrow$) of PrO_2 in the AF1 magnetic phase. The red and blue colors correspond to positive and negative values (± 0.07 electrons/Å^3), respectively. The small red balls are O atoms.

Most calculations were done with the antiferromagnetic phase AF1 which consists of ferromagnetic Pr planes stacked antiferromagnetically with respect to the axis along which the unit cell is doubled (see Fig. 3). Additional calculations were also done for two other magnetic phases for the distorted structure with the lowest energy (which is JT2, see Sec. IV). The first one is AF2, which consists of antiferromagnetic planes stacked antiferromagnetically [see Fig. 10(a) of Ref. 30], and the second one is the ferromagnetic phase (F).

IV. RESULTS AND DISCUSSION

For atoms with a partially filled $4f$ or $5f$ shell, it is a difficult task to find the corresponding electronic configuration which leads to the lowest total energy. The situation can become particularly tricky when an orbital-dependent potential (as, for example, PBE+U) is used since such a potential usually leads to numerous local minima in the electronic configuration space. In the case of PrO_2, already at the PBE level (with an orbital-independent potential), it was possible to stabilize a few different solutions (for a given geometry and magnetic phase) by starting such calculations with different electron densities. For the PBE+U+SO calculations, we considered several starting configurations of the $4f$ electrons. These include the solution(s) obtained by PBE, the crystal field states t_1, t_2, and a_2, and the pure m states satisfying all or some of Hund's rules. We also found slightly different results when we started from PBE calculations, with and without SO coupling, and then used the corresponding occupation matrix and electron density to start the PBE+U+SO calculations.

Among the different PBE+U+SO results, the most stable one was obtained by starting from a PBE+SO solution. Figure 3 shows the corresponding spin magnetization density $\rho_\uparrow - \rho_\downarrow$ (in the AF1 magnetic phase), whose shape is dominated by a single fully spin-polarized localized Pr $4f$ electron. Therefore, the shape of the spin magnetization density reflects the shape of the electron density of this localized $4f$ electron. We can see that each *atomic* spin magnetization density has eight lobes and, in fact, by choosing an appropriate orientation of a local coordinate system to express the Pr $4f$ occupation matrix, the $4f$ electron density roughly corresponds to an electron in an orbital whose angular part is a linear combination of the spherical harmonics $Y_{3,-2}$ and $Y_{3,2}$. Such a local coordinate system would be, for instance, one whose z axis points in the [111] cubic direction. Among the eight lobes, four (those situated in a plane perpendicular to the direction along which the unit cell is doubled) point in a direction such that the oxygen atoms are maximally avoided, whereas the other four (those situated in a plane parallel to the direction along which the unit cell is doubled) point in a direction slightly deviating from a nearest-neighboring oxygen atom. This feature of the electronic structure will be important later on to explain which one of the considered distorted structures [(a)–(d) of Fig. 1] leads to the lowest total energy and largest distortion. All the results discussed below were obtained with this Pr $4f$ electronic configuration.

In Fig. 4, we show the variation of the fundamental band gap Δ, magnetic moments (μ_{tot}, μ_S, and μ_L), distortion d of the oxygen sublattice, and number of $4f$ electrons per Pr atom (within the atomic sphere $R_{\text{MT}}^{\text{Pr}}=2.5$ a.u.) with respect to the Coulomb parameter U_{eff} which was varied between 0 (corresponding to a PBE calculation) and 8 eV. These calculations were done for the JT2 distorted structure (which leads to the lowest total energy, see below) and the AF1 magnetic phase. From Fig. 4(a), we can see that the band gap Δ increases rapidly from 0.09 eV (for $U_{\text{eff}}=0$ eV) to 1.65 eV (for $U_{\text{eff}}=4$ eV), while the increase between $U_{\text{eff}}=4$ and 8 eV is only 0.16 eV. From a simple estimate using our calculated fundamental band gap and the measured activation energy of 0.262 eV for the electrical conductivity,[30] a value for U_{eff} not larger than 0.5 eV seems to be more appropriate. The best agreement is obtained with $U_{\text{eff}}=0.2$ eV (the second data point) which yields $\Delta=0.26$ eV. Nevertheless, the mechanism responsible for the reported conductivity is unknown and different conduction mechanisms (ionic and electronic) were suggested.[30] We would not expect such a small value for U_{eff} for the present system. For instance, for CeO_2 and Ce_2O_3, the best agreement with experiment is obtained for U_{eff} lying in the range 2–5 eV.[9–11] Furthermore, the measured onset of the optical conductivity of $PrO_{2-\delta}$ is $\sim$2 eV,[38]

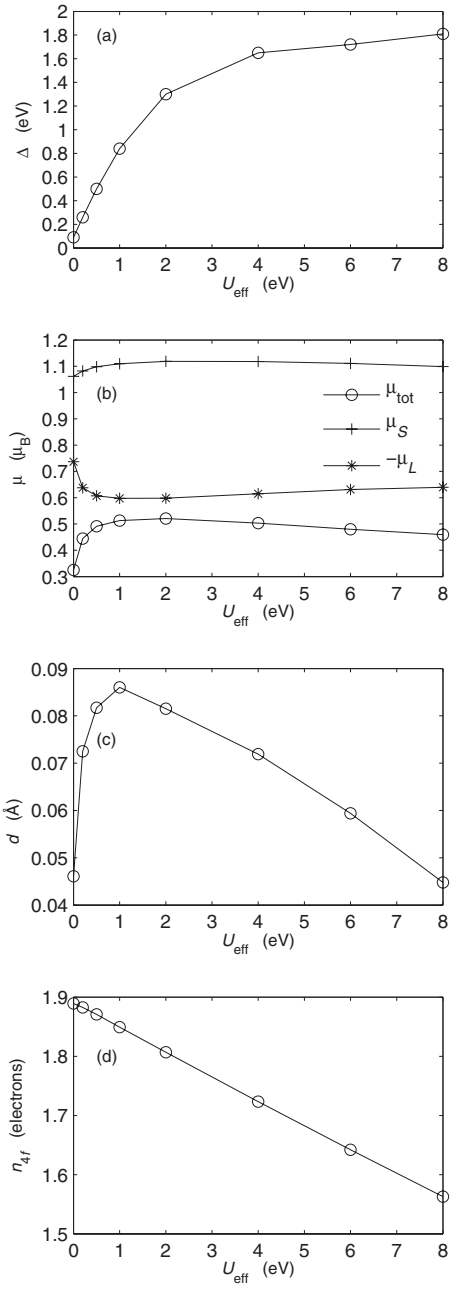

FIG. 4. Variation with respect to the Coulomb parameter U_{eff} is shown for (a) the fundamental band gap, (b) the Pr magnetic moments, (c) the distortion, and (d) the number of $4f$ electrons per Pr atom. These PBE+U+SO results were obtained for the JT2 distorted structure and AF1 magnetic phase. The second and third data points are for U_{eff}=0.2 and 0.5 eV, respectively. The lines between the calculated points are only guides for the eyes.

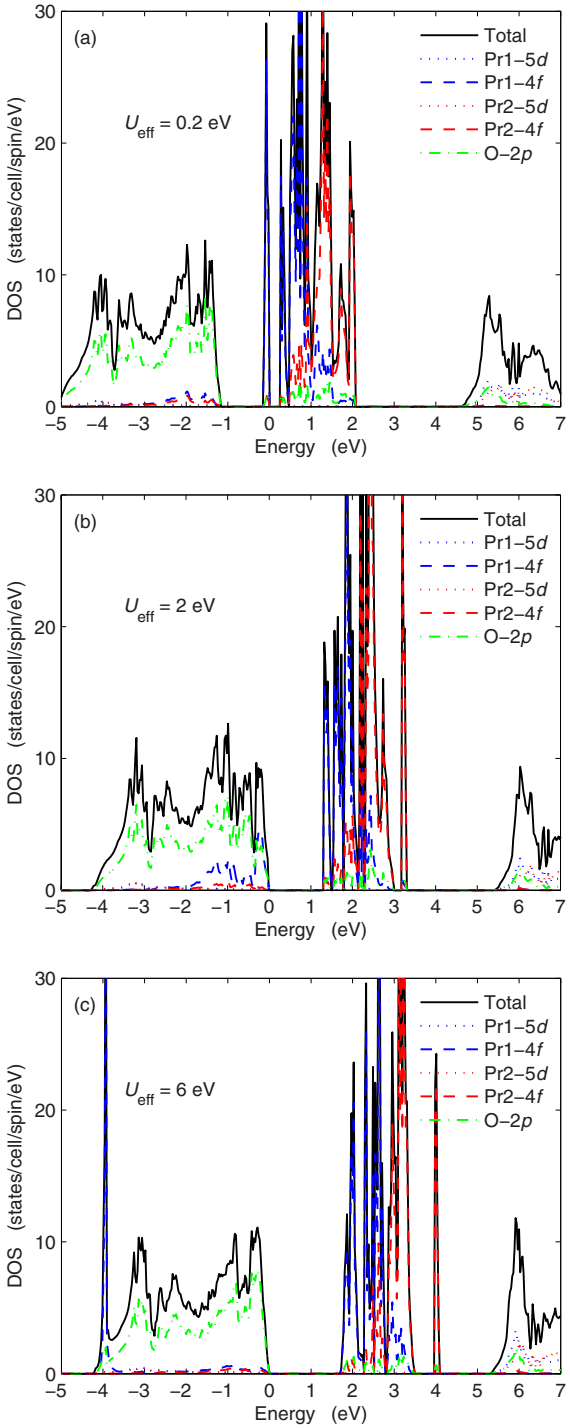

FIG. 5. (Color online) PBE+U+SO spin-up DOS of PrO_2 in the AF1 magnetic phase and JT2 structure for (a) U_{eff}=0.2 eV, (b) U_{eff}=2 eV, and (c) U_{eff}=6 eV. The Fermi energy is set at zero. No broadening was applied.

which is better reproduced with a large value of U_{eff} (see below). Figure 4(b) shows that the total magnetic moment reaches its maximum value (0.52 μ_B) at approximately U_{eff} =2 eV, whereas for U_{eff}=0 eV (PBE only), μ_{tot} would be clearly lower than the experimental values [0.5–0.75 μ_B (Refs. 30, 33, and 41)]. Nevertheless, we recall that an atomic magnetic moment is a quantity for which a unique definition does not exist and that its value depends on the atomic radius R_{MT}. We can also observe that the magnitudes of the spin μ_S and orbital μ_L magnetic moments behave differently with respect to the variation of U_{eff} and that the variation of μ_{tot} is mainly due to the μ_L component. The curve [Fig. 4(c)] for the oxygen distortion d shows, at U_{eff} =1 eV, a maximum of 0.086 Å, which is slightly above the experimental range 0.065–0.078 Å.[30] The best agreement

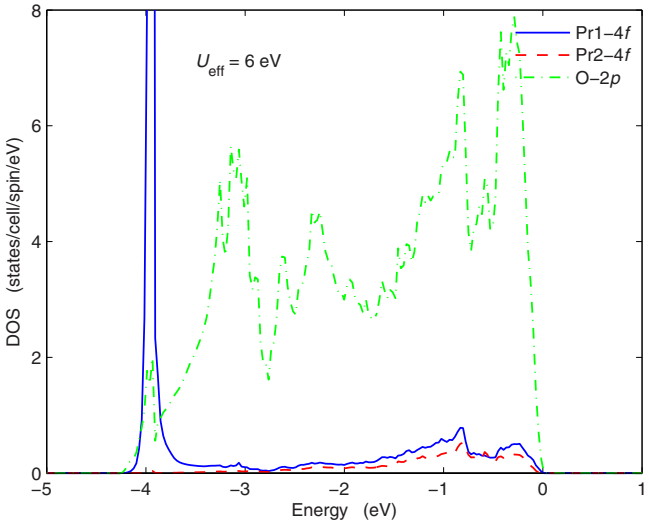

FIG. 6. (Color online) PBE+U+SO spin-up DOS of PrO_2 in the AF1 magnetic phase and JT2 structure for U_{eff}=6 eV. The Fermi energy is set at zero. No broadening was applied.

would be obtained for U_{eff}=0.2 and 4 eV, both yielding d =0.072 Å, while for U_{eff}=0 and 8 eV, $d \sim 0.045$ Å, which is clearly too small compared to experiment. Figure 4(d) shows that the number of 4f electrons per Pr atom n_{4f} decreases linearly with U_{eff} from 1.89 electrons (at U_{eff}=0 eV) to 1.56 electrons (at U_{eff}=8 eV). Assuming the 4f occupancy of 1.5–1.6 electrons calculated in Refs. 35–37 makes a large value of U_{eff} more appropriate.

In order to have more information about a proper value of U_{eff} for PrO_2, we used the method of Anisimov and Gunnarsson[60] (constrained calculation) to calculate U_{eff} in an *ab initio* way [see Ref. 61 for details about the method when used with the FP-(L)APW+lo basis set]. Using this method, we obtained a value of about U_{eff}=7.5 eV, but we want to stress that the calculations had to be done assuming a Pr^{3+} state (i.e., two 4f electrons per Pr atom) since it is not possible to apply this method for less than two 4f electrons.[60,61] Therefore, we can expect the value of U_{eff} to be slightly smaller since in PrO_2 each Pr atom contains about 1.5 electrons. Nevertheless, the result of this *ab initio* calculation of U_{eff} indicates that the use of a large U_{eff} is more appropriate for PrO_2.

In Fig. 5, the density of states (DOS) of the AF1 magnetic phase of PrO_2 in the JT2 distorted structure is plotted, and three values of U_{eff} (0.2, 2, and 6 eV) were chosen in order to show the evolution of the DOS with respect to the increase of U_{eff}. For U_{eff}=0.2 eV [Fig. 5(a)], we can see that the highest occupied states (sharp peak) are of Pr 4f character and are situated about 1 eV above the top of O 2p bands. The fundamental band gap (0.26 eV) separates this sharp occupied Pr 4f peak from the rest of the Pr 4f bands. Then, at about 5 eV above the Fermi energy, states predominantly of Pr 5d character begin to appear. The main effect of increasing U_{eff} is to separate the occupied from the unoccupied Pr 4f states. For U_{eff}=2 eV [Fig. 5(b)], a large part of the occupied Pr 4f states is now situated at the highest O 2p states, which make the top of the valence band having a

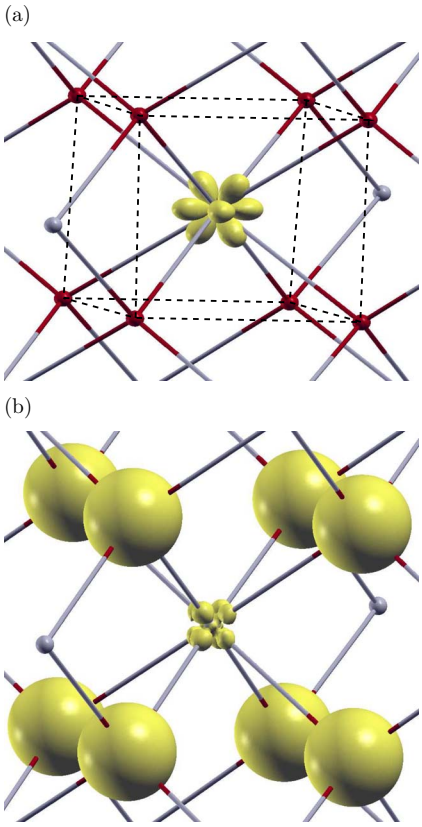

FIG. 7. (Color online) PBE+U+SO (U_{eff}=6 eV) electron density (at an isovalue of 1.1 electrons/Å^3) corresponding to the electronic states (a) at the position of the Pr 4f peak at −4 eV (see Fig. 6) and (b) from the region extending from −3 to 0 eV (see Fig. 6). The electron density is plotted only inside the cube enclosing a Pr atom (the central atom) and its eight nearest-neighboring O atoms.

mixed Pr 4f/O 2p character, where hybridization is evident from the relatively broad 4f partial DOS. Applying U_{eff} =6 eV [Fig. 5(c)] shifts the occupied Pr 4f states down to about 4 eV below the Fermi energy and concentrates them into a sharp peak. The latter corresponds to a single localized 4f electron, while between ~−3 and 0 eV, the integration of the Pr 4f DOS yields about 0.65 4f electrons (spin up plus spin down) in bands of mainly O 2p character. This is shown in more detail in Fig. 6. One can clearly see the peak around −4 eV corresponding to the localized Pr 4f electron. Note that the peak from the O 2p DOS at −4 eV comes from separate bands without 4f contributions and thus these 4f states are localized and not hybridized with the O 2p states. On the other hand, the small Pr 4f DOS in the range −3–0 eV corresponds to hybridized 4f states. A further indication of this Pr 4f/O 2p hybridization can be observed from some similarities in the positions of the peaks at −0.8 and −0.3 eV between the Pr 4f and O 2p curves. Note that the spin-up and spin-down Pr 4f DOSs above −3 eV (i.e., Pr1 4f and Pr2 4f) are very similar.

Figure 7 shows the electron density (spin up plus spin down) of the bands (a) around −4 eV and (b) due to the states within the interval −3–0 eV. The electron density of Fig. 7(a) is very similar to the spin magnetization density (see Fig. 3) due to the full spin polarization of the localized

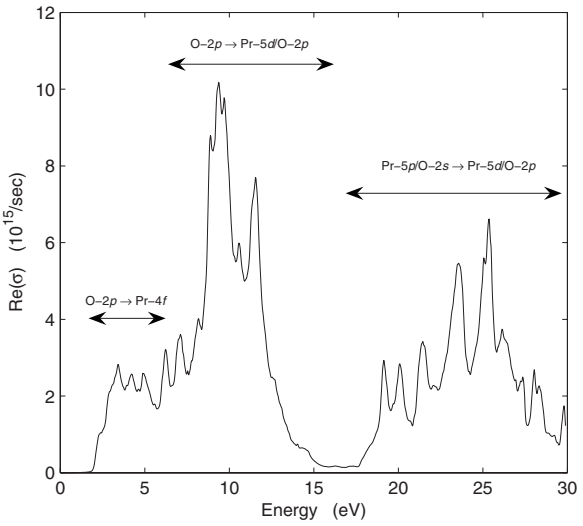

FIG. 8. Real part of the orientationally averaged optical conductivity σ of PrO_2 (AF1 magnetic phase and JT2 distorted structure) obtained with PBE+U+SO (U_{eff}=6 eV). A Lorentzian broadening (Γ=0.03 eV) was applied.

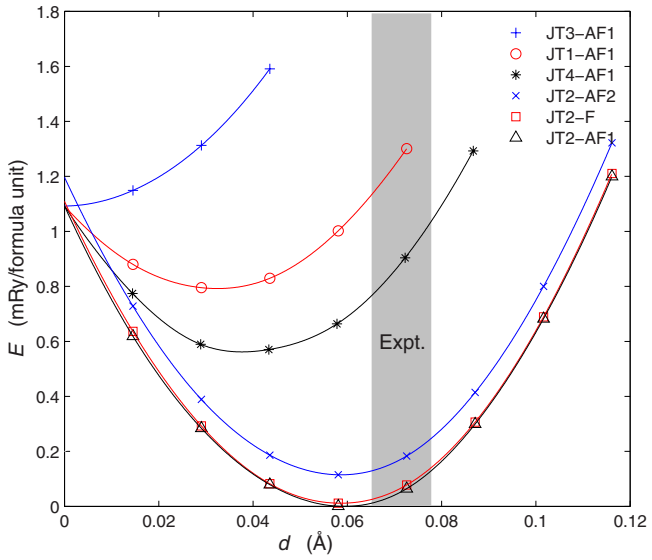

FIG. 9. (Color online) PBE+U+SO (U_{eff}=6 eV) total energy E vs distortion d from the perfect cubic fluorite structure. JT1, JT2, JT3, and JT4 refer to the distorted structures in Fig. 1. AF1 and AF2 refer to the two antiferromagnetic phases considered in this work (see text), and F to the ferromagnetic phase. The minimum of the lowest-energy curve was set at E=0. The range of experimental values is represented by the shaded region. The lines between the calculated points are only guides for the eyes.

$4f$ electron (i.e., the electron density of the other spin is almost negligible). The orientation of the lobes of this localized $4f$ electron is closely related to the Jahn-Teller distortion (discussed below). In Fig. 7(b), a large (spherical) electron density around the O atoms is evident but a small Pr $4f$ density is also visible. The lobes of this $4f$ electron density point toward the O atoms and indicate a small hybridization (bonding) between Pr $4f$ and O $2p$ states in this energy range. Note the different orientations of the lobes coming from the localized [Fig. 7(a)] or hybridized [Fig. 7(b)] $4f$ electrons. The former tend to avoid the O atoms, whereas the latter point toward them.

This picture for the electronic structure of PrO_2 (one localized $4f$ electron plus ~0.65 delocalized $4f$ electron) is consistent with the conclusions drawn from experimental studies.[39,40] Derived from experimental data, van der Kolk and Dorenbos[2] proposed a model to predict the insulating or metallic behavior and chemical stability of lanthanide materials. From their model, it was predicted that for PrO_2, the $4f$ empty states are situated at about 2 eV above the top of the valence band and 4 eV below the $5d$ conduction band, a feature which is quite well reproduced by our calculated DOS.

Figure 8 shows the real part of the optical conductivity which was obtained with U_{eff}=6 eV. The onset of the conductivity at ~2 eV and the position of the most important peaks are in fair agreement with the measured spectrum of $PrO_{2-\delta}$ (Ref. 38). As indicated in Fig. 8, the transitions below 6 eV are mainly from O $2p$ bands (which also contain some Pr $4f$ and Pr $5d$ characters) into Pr $4f$ bands. Between 6 and 16 eV, the transitions are from the O $2p$ bands into bands of mixed Pr $5d$/O $2p$ character, while above 16 eV, the transitions involve the Pr $5p$/O $2s$ occupied and Pr $5d$/O $2p$ unoccupied bands.

The variation of the PBE+U+SO total energy with respect to the oxygen distortion d is shown in Fig. 9 for U_{eff}=6 eV. We can see that three curves have a minimum situated at 0.059 Å (see also Table II) which is only 0.006 Å smaller than the lower bound of the range 0.065–0.078 Å of the experimental values.[30] These three curves correspond to different magnetic phases (AF1, AF2, and F) but all for the JT2 distorted structure. The same minimum value for the distortion d indicates that the magnetic ordering has a negligible influence on the Jahn-Teller effect. This is in accordance with the experimental fact that the Néel temperature T_N=13.5 K is much lower than the distortion temperature of T_D=120 K. The JT2-AF1 and JT2-F curves are nearly indistinguishable (about 0.01 mRy/f.u. of difference at the minimum), while the JT2-AF2 curve is about 0.1 mRy/f.u. higher in energy. Concerning the other distorted structures, the minimum of structures JT1 and JT4 are situated at d =0.032 and 0.038 Å, respectively, which are clearly smaller than the lower bound of the experimental values, while structure JT3 does not distort at all.

The reason why the JT2 structure leads to the largest distortion and lowest total energy is quite simple. As described previously, the Pr $4f$ electron density has eight dominating lobes [see Fig. 3 or 7(a)], four of them (situated within the same plane) pointing approximately in the direction of first-neighboring oxygen atoms. For the JT2 structure, these four lobes point in the directions of the oxygen atoms which correspond to a long Pr–O bond [see Fig. 2(c)], which is the energetically most favorable situation. For the case of the distorted structures JT1 and JT4, this situation happens only for 50% of the Pr atoms, namely, the Pr atoms which are in oxygen cages (a) and (f) of Fig. 2, respectively, while the other 50% Pr atoms are in cages which do not lead to such a

TABLE II. Properties of PrO_2 for several magnetic phases obtained with PBE+U+SO (U_{eff}=6 eV) for the JT2 structure. d (in Å) is the magnitude of the distortion and E (in mRy/f.u.) is the total energy at d (E=0 was set at the minimum of the lowest-energy curve). μ_S, μ_L, and μ_{tot} (in μ_B) are the spin, orbital, and total magnetic moments of Pr atom, and Δ (in eV) is the fundamental band gap.

	d	E	μ_S	μ_L	μ_{tot}	Δ
AF1	0.059	0	1.11	−0.63	0.48	1.7
AF2	0.059	0.11	1.11	−0.62	0.49	1.8
F	0.059	0.01	1.11	−0.62	0.48	1.5
Expt.	0.065–0.078[a]				0.5–0.75[b]	

[a]Reference 30.
[b]References 30, 33, and 41.

favorable situation [(b) and (e) of Fig. 2, respectively]. In the case of structure JT3, such a favorable situation never happens since the corresponding oxygen cage is (d) of Fig. 2, where the four short Pr–O bonds form a tetrahedron.

As already noted above, we can see from Table II that the orbital contribution μ_L to the magnetic moment is important with ~0.6 μ_B and the opposite sign of the spin contribution μ_S. By taking both into account, we find a total magnetic moment μ_{tot} in good agreement with the experimental range 0.5–0.75 μ_B.[30,33,41] Similarly as for the distortion, the magnetic moments and fundamental band gap do not vary much among the different magnetic phases.

V. CONCLUSION

Bulk PrO_2 was studied using the PBE+U functional for the exchange-correlation energy including SO coupling. The influence of the Coulomb parameter $U_{eff}=U-J$ (which was varied from 0 to 8 eV) on the electronic, magnetic, and structural properties was investigated. The results showed that good agreement with experiment can be obtained for the magnetic moment and magnitude of the distortion of the oxygen sublattice for values of U_{eff} situated between 0.2 and 6 eV. U_{eff}=6 eV seems to be a good choice since it leads to qualitative agreement with the experiment for the electronic structure and is relatively close to the *ab initio* value of U_{eff} which was obtained from a constrained calculation. Nevertheless, U_{eff}=6 eV leads to a magnitude for the distortion from the cubic fluorite structure which is slightly smaller than the reported experimental value, while a perfect agreement can be obtained with, e.g., U_{eff}=0.2 or 4 eV. With U_{eff}=6 eV, about 1.65 4f electrons (one localized plus 0.65 delocalized) per Pr atom are found, which means that the Pr ions are intermediate between trivalent Pr^{3+} and tetravalent Pr^{4+}. We also studied the effects of the long-range magnetic ordering on the calculated properties but found them not to be important. These results were obtained for the distorted structure JT2, which has the lowest total energy among the four models of distortion we considered. Therefore, our calculations strongly support the JT2 structure over the other distortion models considered. Only for this case we obtain results that are consistent with the available experimental data.

Note added in proof. Recently we became aware of two papers by Webster *et al.*[63] (x-ray diffraction experiment) and Jensen[64] (theoretical calculations using a model Hamiltonian) on PrO_2. In both Refs. 63 and 64 it is concluded that the distorted structure JT2 is the correct one, which is in accordance with our results.

ACKNOWLEDGMENTS

This work was supported by the Austrian Grid project (WP A-7). We also thank Robert Laskowski for useful discussions.

[1] G. Adachi and N. Imanaka, Chem. Rev. (Washington, D.C.) **98**, 1479 (1998).
[2] E. van der Kolk and P. Dorenbos, Chem. Mater. **18**, 3458 (2006).
[3] P. Hohenberg and W. Kohn, Phys. Rev. **136**, B864 (1964).
[4] W. Kohn and L. J. Sham, Phys. Rev. **140**, A1133 (1965).
[5] S. Fabris, S. de Gironcoli, S. Baroni, G. Vicario, and G. Balducci, Phys. Rev. B **71**, 041102(R) (2005); G. Kresse, P. Blaha, J. L. F. Da Silva, and M. V. Ganduglia-Pirovano, *ibid.* **72**, 237101 (2005); S. Fabris, S. de Gironcoli, S. Baroni, G. Vicario, and G. Balducci, *ibid.* **72**, 237102 (2005).
[6] L. Gerward, J. Staun Olsen, L. Petit, G. Vaitheeswaran, V. Kanchana, and A. Svane, J. Alloys Compd. **400**, 56 (2005).
[7] Y. Jiang, J. B. Adams, and M. van Schilfgaarde, J. Chem. Phys. **123**, 064701 (2005).
[8] P. J. Hay, R. L. Martin, J. Uddin, and G. E. Scuseria, J. Chem. Phys. **125**, 034712 (2006).
[9] D. A. Andersson, S. I. Simak, B. Johansson, I. A. Abrikosov, and N. V. Skorodumova, Phys. Rev. B **75**, 035109 (2007).
[10] C. Loschen, J. Carrasco, K. M. Neyman, and F. Illas, Phys. Rev. B **75**, 035115 (2007).
[11] J. L. F. Da Silva, M. V. Ganduglia-Pirovano, J. Sauer, V. Bayer, and G. Kresse, Phys. Rev. B **75**, 045121 (2007).
[12] J. P. Perdew and A. Zunger, Phys. Rev. B **23**, 5048 (1981).
[13] V. I. Anisimov, J. Zaanen, and O. K. Andersen, Phys. Rev. B **44**,

943 (1991).
[14] V. I. Anisimov, F. Aryasetiawan, and A. I. Lichtenstein, J. Phys.: Condens. Matter **9**, 767 (1997).
[15] R. Laskowski, G. K. H. Madsen, P. Blaha, and K. Schwarz, Phys. Rev. B **69**, 140408(R) (2004).
[16] D. Torumba, V. Vanhoof, M. Rots, and S. Cottenier, Phys. Rev. B **74**, 014409 (2006).
[17] P. Larson, W. R. L. Lambrecht, A. Chantis, and M. van Schilfgaarde, Phys. Rev. B **75**, 045114 (2007).
[18] H. Y. Geng, Y. Chen, Y. Kaneta, and M. Kinoshita, Phys. Rev. B **75**, 054111 (2007).
[19] A. D. Becke, J. Chem. Phys. **98**, 1372 (1993).
[20] A. D. Becke, J. Chem. Phys. **98**, 5648 (1993).
[21] K. N. Kudin, G. E. Scuseria, and R. L. Martin, Phys. Rev. Lett. **89**, 266402 (2002).
[22] I. D. Prodan, G. E. Scuseria, J. A. Sordo, K. N. Kudin, and R. L. Martin, J. Chem. Phys. **123**, 014703 (2005).
[23] I. D. Prodan, G. E. Scuseria, and R. L. Martin, Phys. Rev. B **73**, 045104 (2006).
[24] I. D. Prodan, G. E. Scuseria, and R. L. Martin, Phys. Rev. B **76**, 033101 (2007).
[25] A. Svane, W. M. Temmerman, Z. Szotek, J. Lægsgaard, and H. Winter, Int. J. Quantum Chem. **77**, 799 (2000).
[26] L. Petit, A. Svane, Z. Szotek, and W. M. Temmerman, Phys. Rev. B **72**, 205118 (2005).
[27] L. Petit, A. Svane, Z. Szotek, and W. M. Temmerman, Top. Appl. Phys. **106**, 331 (2007).
[28] J. P. Perdew, K. Burke, and M. Ernzerhof, Phys. Rev. Lett. **77**, 3865 (1996); **78**, 1396(E) (1997).
[29] A. T. Boothroyd, C. H. Gardiner, S. J. S. Lister, P. Santini, B. D. Rainford, L. D. Noailles, D. B. Currie, R. S. Eccleston, and R. I. Bewley, Phys. Rev. Lett. **86**, 2082 (2001).
[30] C. H. Gardiner, A. T. Boothroyd, P. Pattison, M. J. McKelvy, G. J. McIntyre, and S. J. S. Lister, Phys. Rev. B **70**, 024415 (2004).
[31] C. H. Gardiner, A. T. Boothroyd, M. J. McKelvy, G. J. McIntyre, and K. Prokeš, Phys. Rev. B **70**, 024416 (2004).
[32] G. Bevilacqua, D. Ippolito, and L. Martinelli, Phys. Rev. B **69**, 155208 (2004).
[33] S. Kern, C.-K. Loong, J. Faber, Jr., and G. H. Lander, Solid State Commun. **49**, 295 (1984).
[34] S. Kern, C.-K. Loong, and G. H. Lander, Phys. Rev. B **32**, 3051 (1985).
[35] A. Bianconi, A. Kotani, K. Okada, R. Giorgi, A. Gargano, A. Marcelli, and T. Miyahara, Phys. Rev. B **38**, 3433 (1988).
[36] H. Ogasawara, A. Kotani, K. Okada, and B. T. Thole, Phys. Rev. B **43**, 854 (1991).
[37] S. M. Butorin, L.-C. Duda, J.-H. Guo, N. Wassdahl, J. Nordgren, M. Nakazawa, and A. Kotani, J. Phys.: Condens. Matter **9**, 8155 (1997).
[38] S. Kimura, F. Arai, and M. Ikezawa, J. Electron Spectrosc. Relat. Phenom. **78**, 135 (1996).
[39] R. C. Karnatak, J.-M. Esteva, H. Dexpert, M. Gasgnier, P. E. Caro, and L. Albert, Phys. Rev. B **36**, 1745 (1987).
[40] H. Dexpert, R. C. Karnatak, J.-M. Esteva, J. P. Connerade, M. Gasgnier, P. E. Caro, and L. Albert, Phys. Rev. B **36**, 1750 (1987).
[41] C. H. Gardiner, A. T. Boothroyd, S. J. S. Lister, M. J. McKelvy, S. Hull, and B. H. Larsen, Appl. Phys. A: Mater. Sci. Process. **74**, S1773 (2002).
[42] M. McKelvy and L. Eyring, J. Cryst. Growth **62**, 635 (1983).
[43] D. D. Koelling, A. M. Boring, and J. H. Wood, Solid State Commun. **47**, 227 (1983).
[44] J. Dąbrowski, V. Zavodinsky, and A. Fleszar, Microelectron. Reliab. **41**, 1093 (2001).
[45] S. Mehrotra and A. K. Bandyopadhyay, J. Alloys Compd. **436**, 56 (2007).
[46] M. Diviš, J. Rusz, and V. Nekvasil, Czech. J. Phys. **54**, D291 (2004).
[47] M. Diviš and J. Rusz, J. Magn. Magn. Mater. **290-291**, 1015 (2005).
[48] P. Novák and M. Diviš, Phys. Status Solidi B **244**, 3168 (2007).
[49] L.-G. Liu, Earth Planet. Sci. Lett. **49**, 166 (1980).
[50] P. Blaha, K. Schwarz, G. K. H. Madsen, D. Kvasnicka, and J. Luitz, *WIEN2K: An Augmented Plane Wave and Local Orbitals Program for Calculating Crystal Properties*, edited by K. Schwarz (Vienna University of Technology, Austria, 2001).
[51] J. Schweifer, P. Blaha, and K. Schwarz, in *2nd Austrian Grid Symposium*, edited by J. Volkert, T. Fahringer, D. Kranzlmüller, and W. Schreiner (Austrian Computer Society, Vienna, 2007), p. 179.
[52] The jobs were managed by W2GRID, a Perl based middleware for grid computing, which allows to submit a job which is automatically migrated to the most suitable computer resource (cluster) and is executed there (see http://www.w2grid.at).
[53] D. J. Singh, *Planewaves, Pseudopotentials and the LAPW Method* (Kluwer Academic, Boston, 1994).
[54] E. Sjöstedt, L. Nordström, and D. J. Singh, Solid State Commun. **114**, 15 (2000).
[55] D. D. Koelling and B. N. Harmon, J. Phys. C **10**, 3107 (1977).
[56] A. H. MacDonald, W. E. Pickett, and D. D. Koelling, J. Phys. C **13**, 2675 (1980).
[57] J. Kuneš, P. Novák, M. Diviš, and P. M. Oppeneer, Phys. Rev. B **63**, 205111 (2001).
[58] A. I. Liechtenstein, V. I. Anisimov, and J. Zaanen, Phys. Rev. B **52**, R5467 (1995).
[59] V. I. Anisimov, I. V. Solovyev, M. A. Korotin, M. T. Czyżyk, and G. A. Sawatzky, Phys. Rev. B **48**, 16929 (1993).
[60] V. I. Anisimov and O. Gunnarsson, Phys. Rev. B **43**, 7570 (1991).
[61] G. K. H. Madsen and P. Novák, Europhys. Lett. **69**, 777 (2005).
[62] A. B. Shick, A. I. Liechtenstein, and W. E. Pickett, Phys. Rev. B **60**, 10763 (1999).
[63] C. H. Webster, L. M. Helme, A. T. Boothroyd, D. F. McMorrow, S. B. Wilkins, C. Detlefs, B. Detlefs, R. I. Bewley, and M. J. McKelvy, Phys. Rev. B **76**, 134419 (2007).
[64] J. Jensen, Phys. Rev. B **76**, 144428 (2007).